Crystallization Kinetics of the Pure Triacylglycerols Glycerol-1,3-Dipalmitate-2-Oleate, Glycerol-1-Palmitate-2-Oleate-3-Stearate, and Glycerol-1,3-Distearate-2-Oleate

Ph. Rousset* and M. Rappaz

Laboratoire de Métallurgie Physique, Ecole Polytechnique Fédérale de Lausanne, MX-G, CH-1015 Lausanne, Switzerland

ABSTRACT: Crystallization kinetics of the three main components of cocoa butter, the triacylglycerols POP, POS, and SOS (where P, O, and S stand for palmitic, oleic, and stearic acids, respectively) were studied by combined differential scanning calorimetry and polarized light microscopy. The morphologies, nucleation kinetics, growth kinetics, and phases of the grains formed were identified with this system. The experimental data, as well as two different models to simulate crystallization and to predict behavior of the pure triacylglycerols, are presented. The first model is based on a macroscopical approach to solidification by using time–temperature–transformation (TTT) diagrams and the additivity principle. It allows prediction of the proportion of the different phases formed for any given thermal path imposed on the sample once the TTT diagram is known for the product. It is illustrated for SOS at constant cooling rates and is compared with experimental results. The second model directly simulates growth of the spherulites in the sample by using nucleation and growth rates that are determined experimentally. It provides a view of the structure as it would be observed with a microscope and shows evolution of the heat released in the sample. Isothermal solidification of POP at 15°C is displayed. The experiment and the model are in good agreement.
JAOCS 73, 1051–1057 (1996).

KEY WORDS: Crystallization kinetics, differential scanning calorimetry, modeling, polarized light microscopy, POP, POS, solidification, SOS, triacylglycerol.

Cocoa butter is composed of about 97% triacylglycerols (TAG), mainly of the type saturated–unsaturated–saturated (1). Among them, the three components glycerol-1,3-dipalmitate-2-oleate (POP), glycerol-1-palmitate-2-oleate-3-stearate (POS), and glycerol-1,3-distearate-2-oleate (SOS) represent between 80 and 90% of the total (2). Because of the polymorphism of these TAG over a narrow temperature range, cocoa butter must be tempered carefully to obtain the desired stable phase in the end product (2,3). To eliminate the added complexity that arises because cocoa butter is a mixture (melting temperature range, microsegregation of the species), this study is focused on the polymorphism and associated crystallization kinetics of the three pure TAG species, POP, POS, and SOS (4). Sato and co-workers (5,6) have investigated the crystallization kinetics of pure TAG during isothermal holding. They identified the beginning of liquid–solid transformation in connection with the phase formed and the pretreatment imposed on the sample (i.e., TAG directly solidified from the melt or mediated *via* an intermediate passage through another, less stable phase). These authors used an optical system with a temperature-controlled cell, which could measure the induction time for solid-phase formation. In the present investigation, differential scanning calorimetry (DSC) and polarized light microscopy (PLM) observations were made simultaneously to obtain a detailed view of crystallization kinetics, grain morphology, and the crystalline phases formed. Indeed, these two methods are complementary. The position and shape of the DSC peaks allow the phases to be identified and the evolution of the volume fraction of solid to be measured. Visual observation gives information on the density, morphology, and growth rate of the grains, provided they are distinct and sufficiently large under the microscope.

After briefly describing the DSC–PLM experimental setup, the first part of this paper is dedicated to the experimental results obtained for the isothermal solidification of POP, POS, and SOS (phases formed, grain morphology, nucleation, and growth kinetics). In the second part, these results are interpreted with models derived from metallurgical studies, namely time–temperature–transformation (TTT) diagrams (7), based upon Avrami-type curves (8) and stochastic nucleation-growth models, which consider the grains as individual entities (9).

EXPERIMENTAL PROCEDURES

Pure TAG (POP, POS, and SOS) were purchased from Larodan (Malmö, Sweden) and had a purity of 99%. Crystallization kinetics of these TAG were investigated by DSC measurements in two different instruments—a Perkin Elmer (Norwalk, CT) DSC-7 and a Mettler FP900 (Mettler A.G., Greifensee, Switzerland). The second instrument allowed an *in situ* observation of the grains under a polarized-light microscope linked to a video recording system. The samples analyzed had a mass between 0.5 and 3 mg with both systems.

*To whom correspondence should be addressed.

They were placed in small pans made of aluminum or glass for the DSC-7 and FP900 instruments, respectively.

The specimens were solidified under isothermal conditions. After heating at 100°C for at least 3 min to ensure complete melting and to "erase" any previous structure of the molecules (10), the specimens were rapidly cooled (50°C/min with the DSC-7, 10°C/min with the FP900) to the desired solidification temperature, T_{iso}, and allowed to solidify. An exothermal peak was measured (liquid to some phase φ), starting at time t_s, and finishing at time t_f. After complete solidification, the specimens were heated slowly at 5°C/min, and an endothermic peak, corresponding to melting of the solidified phase φ, was measured. This peak occurred at a temperature of melting, T_f, which could easily be identified. The integrals of the exothermal and endothermal peaks, ΔH_s and ΔH_f, correspond to the enthalpies of solidification and fusion, respectively.

The phase φ, formed during isothermal holding, was identified by comparing the experimentally determined values of ΔH_s, ΔH_f, and T_f with those previously reported by Sato and co-workers (11,12). On the isothermal plateau, the evolution of the volume fraction of solid, $f_s(t)$, was deduced from the exothermal peak by integration, after numerical treatment. The times t_s and t_f, used to construct the TTT diagrams, were determined as the times at which the volume fraction of solid equaled 1 and 99%, respectively.

PLM observations were used to identify crystal morphologies and to measure the density and growth rate of the grains as a function of undercooling (i.e., the temperature difference between the equilibrium melting point of phase φ and temperature T_{iso}).

EXPERIMENTAL RESULTS

Grain morphology and structure. A detailed solidification model (13,14) requires that several entities be known—the nucleation rate and the growth rate as a function of undercooling, the solid–liquid interfacial area, and the grain morphology. Morphologies of the TAG grains can be quite diversified, as observed in previous studies carried out on cocoa butter (1,15) and tripalmitin (16). Similar morphologies have been observed for POP, POS, and SOS. Four typical ones are shown in Figure 1. In Figure 1A, the grains are spherulitic and appear with a typical dark cross inside. (There are also a few bubbles of air in this micrograph; their borders are much thicker than those of the spherulites.) These spherulites clearly appear homogeneously in the liquid and, up to a certain size, they can move. In Figure 1B, the TAG solidifies as a "mass," which seems to grow from the side of the specimen toward the center (i.e., from right to left in this figure). It is similar to a columnar front of solidification growing inwards in the plane of observation. Figure 1C shows that, at some temperatures, spherulites can coexist with the mass. Finally, in Figure 1D, needle-shaped crystals are shown.

Figure 2 summarizes the various grain morphologies and phases observed for the three TAG investigated as a function

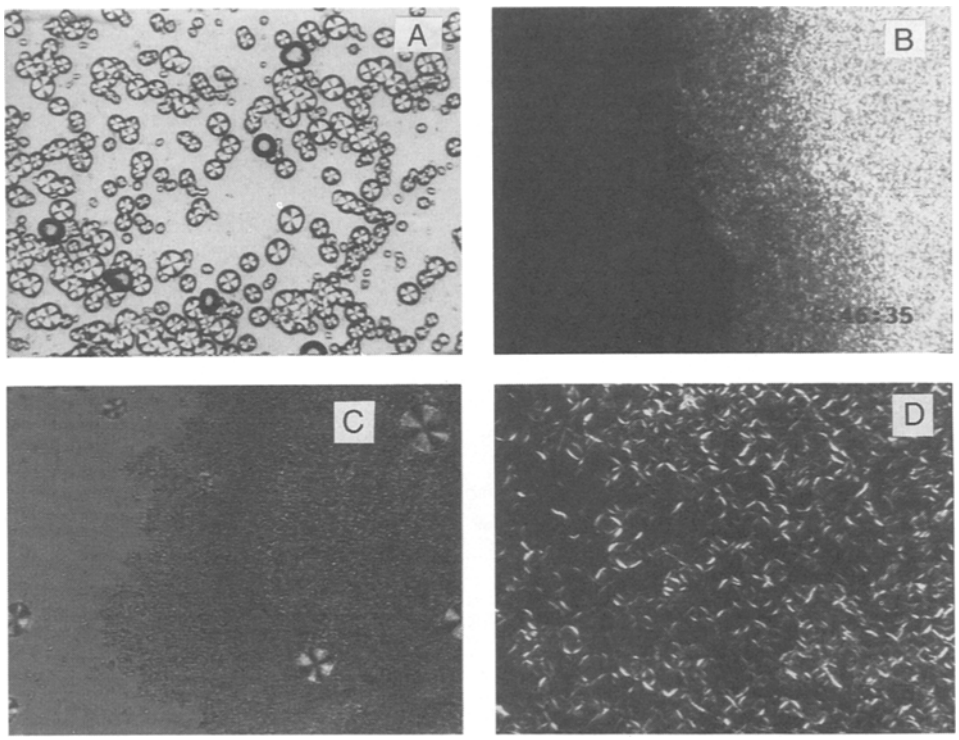

FIG. 1. Morphologies observed: A, spherulites [glycerol-1,3-dipalmitate-2-oleate (POP) at 16°C]; B, mass (POP at 20°C); C, mixture of mass and spherulites (POP at 17°C); and D, needle-like crystals [glycerol-1,3-distearate-2-oleate (SOS at 21°C].

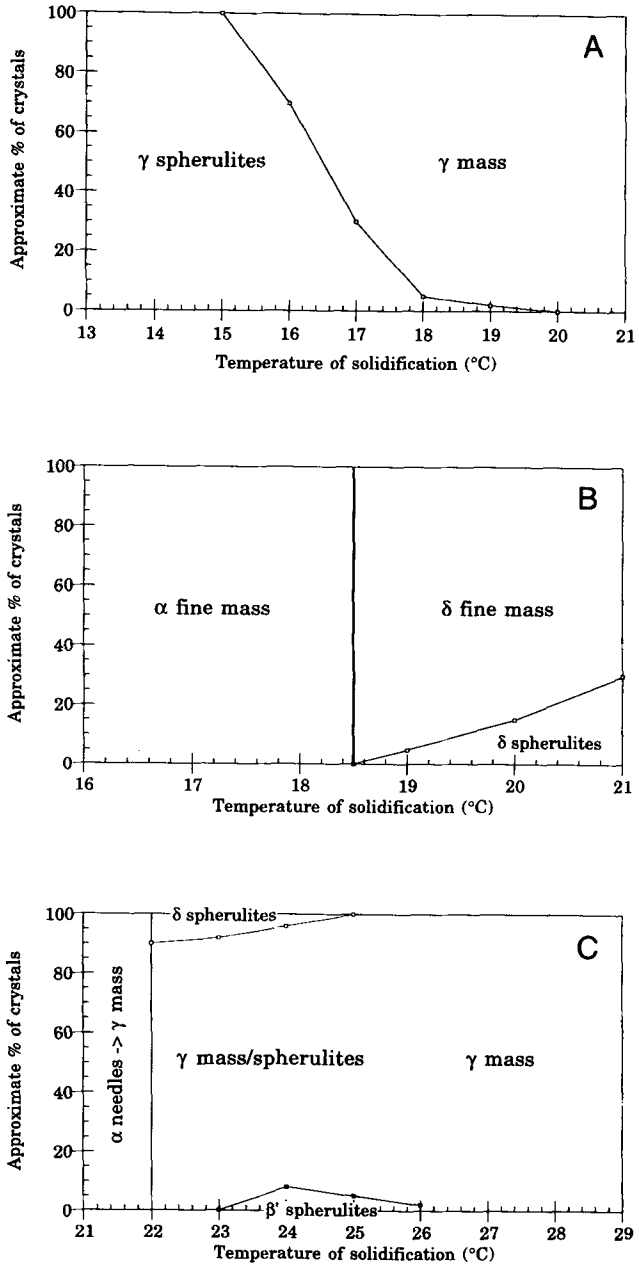

FIG. 2. Approximate volume fractions of the various grain morphologies and crystalline phases for: A, POP; B, glycerol-1-palmitate-2-oleate-3-stearate (POS); C, SOS. Abbreviations as in Figure 1.

of temperature. These latter values are listed in Table 1, together with those of Sato and co-workers (11,12), which are used for identification. The error given for each value corresponds to the standard deviation deduced from similar experiments on both instruments (DSC-7 and FP900).

For POP (Fig. 2A), only the γ-phase forms between 13 and 21°C. At low temperatures, this phase appears in the form of spherulitic grains (Fig. 1A), whereas above 17°C it mainly consists of a continuous mass (Fig. 1B). In between, spherulites and mass coexist with a final volume fraction of

TABLE 1
Properties of the Solid Phases of POP, POS, and SOS[a]

Phase	Temperature of fusion (°C)	Heat of fusion/ solidification (J/g)
POP-γ	23.9 ± 0.6 (27)	98 ± 6 (111)
POS-α	18.9 ± 0.4 (19.5)	73 ± 9 (48)
POS-δ	28.6 ± 0.5 (28.3)	111 ± 11 (104)
SOS-α	22.4 ± 0.4 (23.5)	60 ± 2 (54)
SOS-δ	28.8 ± 0.8	98 ± 20
SOS-γ	35.5 ± 0.3 (35.4)	113 ± 2 (111)

[a]Results in parentheses are from Sato *et al.* (11) and Arishma *et al.* (12). POP, glycerol-1,3-dipalmitate-2-oleate; POS, glycerol-1-palmitate-2-oleate-3-stearate; SOS, glycerol-1,3-distearate-2-oleate.

each morphology given by the curve shown in Figure 2A. In the DSC-7 instrument, some α-phase forms below 14°C, but it rapidly transforms into γ.

Below 18.5°C, POS solidifies as a finely dispersed mass of the α-phase (Fig. 2B). Above this temperature, the δ-phase forms, first as a mass, but then with an increasing number of spherulites as the isothermal temperature is raised. The sharp transition between α and δ is shifted to a lower value (about 17°C) when the specimen is placed in an aluminum pan (DSC-7). A slightly lower enthalpy of fusion for the α-phase was measured, compared with the value reported by Arishima and co-workers (12).

Three morphologies and four phases have been observed for SOS (Fig. 2C). At low temperatures, the α-phase seems to form as needle-shaped crystals (Fig. 1D), but it rapidly transforms into a mass of the γ-phase. Above 21.5°C, several phases can coexist at a given temperature—SOS solidifies essentially into the γ-phase in the form of spherulites or of a continuous mass at low/high temperatures, respectively, together with a small proportion of spherulites of δ and/or β′. Unlike POP, the transition of γ-SOS from one morphology to another is not well defined, and no clear percentage of each phase could be definitely ascertained. The δ-phase observed for SOS has a melting temperature and enthalpies of fusion/solidification that could not be identified with any value previously reported by Sato *et al.* (11) for this TAG. Although its crystallographic structure was not identified in the present investigation, it was named δ to distinguish it from the other phases already observed for SOS. The β′-phase could not be identified from the DSC measurement because only one peak of fusion, whose position and surface were attributed to γ, was observed. However, between 24 and 26°C, scattered spherulites appear among the mass of γ, which were attributed to β′ because, on reheating, they could be seen under the microscope to melt a few seconds later than the mass (β′ has a melting point of 36.5°C, a value slightly higher than the 35.5°C of γ).

TTT diagrams. TTT diagrams were constructed for the three TAG (Fig. 3 for the FP900 experiments and Fig. 4 for the DSC-7 experiments). Such diagrams can be read on horizontal lines, i.e., isothermally at any given temperature: the first point (open symbol) corresponds to the start time (f_s =

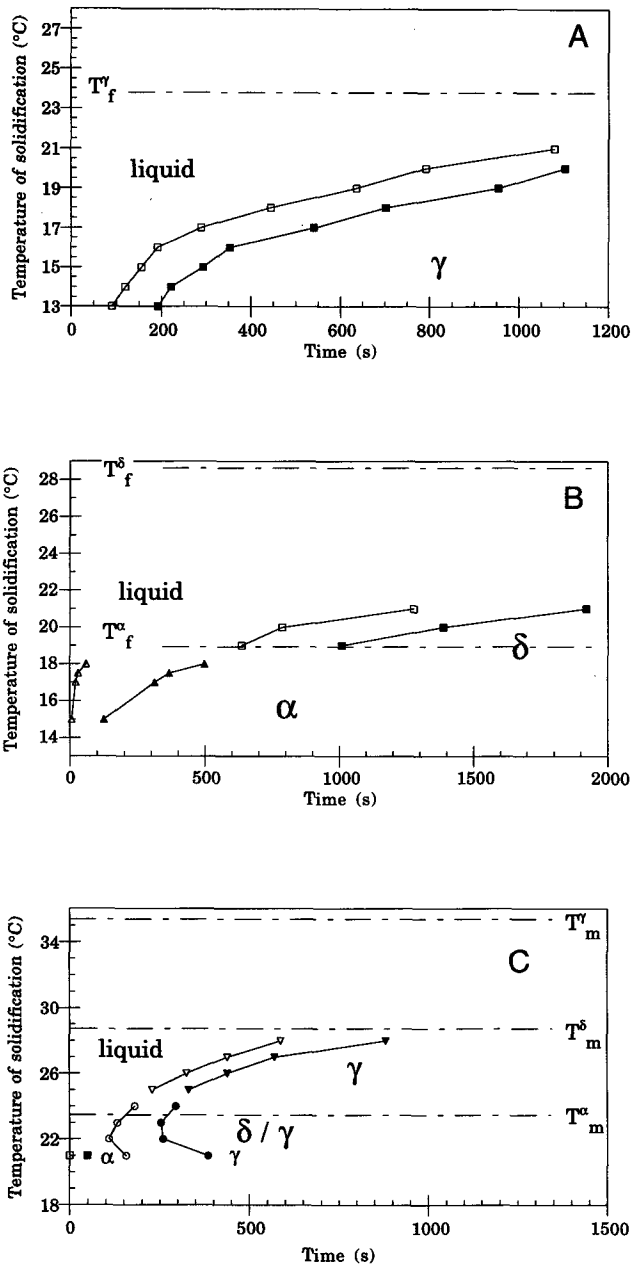

FIG. 3. Time–temperature–transformation diagrams constructed from the FP900 experiments: A, POP; B, POS; and C, SOS. Abbreviations as in Figures 1 and 2.

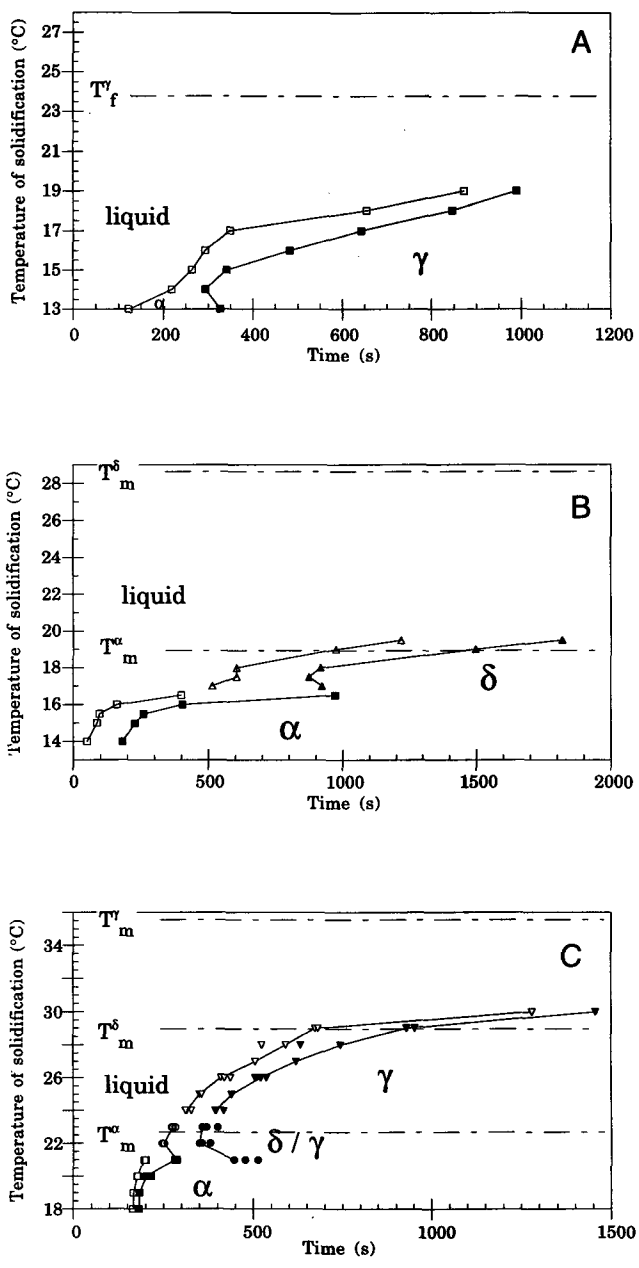

FIG. 4. Time–temperature–transformation diagrams constructed from the DSC-7 (Perkin Elmer, Norwalk, CT) experiments: A, POP; B, POS; and C, SOS. Abbreviations as in Figures 1 and 2.

0.01) of the transformation, whereas the end is reached at the second point ($f_s = 0.99$, filled symbol). They can also be used for any cooling curve by using an additivity principle (17).

The temperature range investigated was selected so that the DSC peak would be observed within a time limit of about 30 min. The temperatures of fusion of the different phases are shown as dashed horizontal lines. As expected, the crystallization kinetics are faster as the temperature is decreased—both the start time, t_s, and the solidification time, $(t_f - t_s)$, are reduced. The crystallization kinetics are slightly faster in the FP900 instrument (glass pans) compared to the DSC-7 (aluminum pans). Also, with the FP900, most of the less stable phases of the three TAG were observed to form and to grow up to higher temperatures.

Nucleation and growth rate of spherulitic grains. Spherulitic grains can be clearly isolated in PLM photographs (Fig. 1A). Under such conditions, the density of grains and the evolution of their radii can be measured as a function of time. Derivatives of these two entities, namely the nucleation rate and the growth rate, are necessary for a detailed model of solidification (see next section). However, the nucleation rate (i.e., time derivative of the grain density) is not easily accessible because the grains must have a minimum size before being observed under the microscope. A simplification was

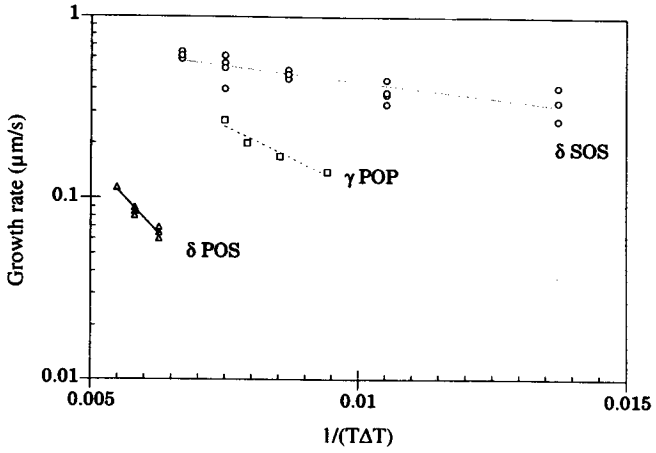

FIG. 5. Growth rate of the spherulites of γ POP, δ POS, and δ SOS. Abbreviations as in Figures 1 and 2.

made for simulation of solidification of POP at 15°C; the final number of grains at the end of solidification was measured, and it was then assumed that all these grains nucleated instantaneously. This instantaneous nucleation model could be refined based upon the shape of the grain boundaries observed at the end of solidification (18).

Because the growth kinetics of the grains is primarily dictated by attachment of the molecules to the existing solid, it can reasonably be assumed that the growth rate, $G(T)$, is the same for all grains and depends only on the temperature. $G(T)$ was estimated by averaging the evolution of the radii of several grains. Results obtained for the spherulitic growth of POP, POS, and SOS are shown as a function of $(T\Delta T)^{-1}$ in Figure 5, where ΔT is the undercooling, i.e., the difference between the equilibrium melting temperature of the corresponding phase and the temperature of solidification. The growth rate kinetics of all three TAG follow the relationship $G(T) = K_1 \exp [-(K_2/T\Delta T)]$ fairly well, which is typical of secondary nucleation mechanisms (19,20). The growth rates of δ-POS, γ-POP, and δ-SOS spherulites are spread over one order of magnitude for the same undercooling. The fastest growth kinetics occur for SOS, which is the most symmetrical molecule. POS has the lowest symmetry among the three molecules and the slowest growth kinetics. Further work would be needed to fully understand these different crystallization kinetics.

MODELING RESULTS

Use of TTT diagrams for nonisothermal crystallization. Evolution of the volume fraction of solid, $f_s(t)$, was directly obtained from integration of the DSC peak and was fitted with an Avrami-type law: $f_s(t) = 1 - \exp(-bt^n)$. $b(T)$ and $n(T)$ are two temperature-dependent parameters. An additivity principle has been developed (17,21) to use TTT diagrams for any cooling cycle. This is based upon decomposition of the cooling curve into small steps where the temperature is held constant. At the beginning of time step i, the volume fraction of solid, $f_{s,i}$, is known from the previous time step, together with the actual temperature, T_i. A fictitious time, θ_i, is introduced so that :

$$f_{s,i} = 1 - \exp\left[-b(T_i)\theta_i^{n(T_i)}\right] \quad [1]$$

The new volume fraction of solid, $f^*_{s,i}$ at the end of this small time step, δt, is then updated according to:

$$f^*_{s,i} = 1 - \exp\left[-b(T_i)\left(\theta_i + \delta t\right)^{n(T_i)}\right] \quad [2]$$

Based upon this principle, a calculation was made, assuming a constant cooling rate, Ṫ, of an SOS specimen. The specimen being small, it was assumed that its temperature was uniform. From the TTT diagram data in Figure 4C and the model, the calculated times of start, t_s, and finish, t_f, of the crystallization are plotted in Figure 6 as a function of the cooling rate. These times are represented as open and filled square symbols, respectively. They can be compared with the DSC-7 measurements made at various cooling rates ranging from −0.05 to −1°C/min (open and filled diamonds, respectively). The melt was held at 100°C for a few minutes prior to cooling, as for the isothermal solidification experiments presented in the previous section. It was quenched at 50°C/min to 30°C and then subsequently allowed to solidify at the corresponding cooling rate, down to a minimum temperature of 24°C. The triangles (corner or base up) in Figure 6 correspond to the simulations and experiments in which this minimum temperature was reached before solidification could start. Calculated and measured start/finish times are in fairly good agreement. In particular, the slowest crystallization kinetics measured at a low cooling rate are correctly reproduced by the additivity principle.

Nucleation-growth model for spherulitic growth. Because TTT diagrams combine in a single set of curves the various contributions of nucleation, growth, and impingement of the grains, they are of particular relevance when these contributions cannot be analyzed separately (e.g., continuous mass). For spherulites, however, a more fundamental analysis can be made with a model previously developed for polymers (13) and metals (14). Assuming that the grains are spherical and

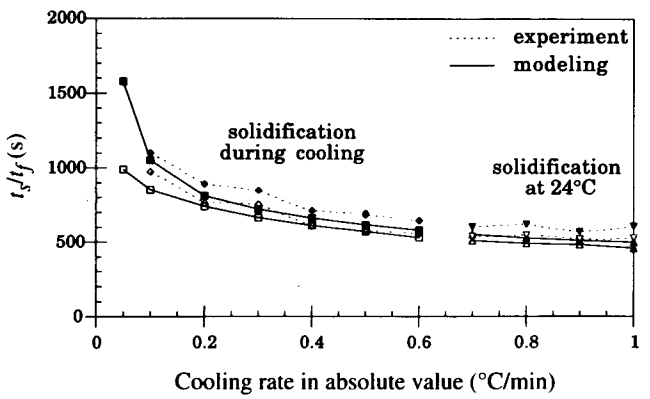

FIG. 6. Influence of the cooling rate between 30 and 24°C on the solidification time of SOS. Comparison between experiment and modeling. Abbreviations as in Figures 1 and 2.

randomly distributed in space, the evolution of the volume fraction of solid fraction is given by the convolution (8):

$$f_s(t) = 1 - \exp[-f_{s,e}(t)] \quad \text{with} \quad f_{s,e}(t) = \int_0^t \dot{n}(\tau) \cdot V(t,\tau) \cdot d\tau \quad [3]$$

where $\dot{n}(\tau)$ is the nucleation rate at time τ, $V(t,\tau)$ is the extended volume of a grain nucleated at time τ and observed at time t. For spherical grains growing at a constant growth rate G, $V(t,\tau)$ would be the volume of a sphere of radius $G \cdot (t - \tau)$, i.e., $V(t,\tau) = \frac{4}{3}\pi[G(t - \tau)]^3$. The extended volume fraction of solid, $f_{s,e}(t)$, is defined as the fraction of solid that would have been obtained if the grains did not impinge on each other.

Equation 3 applies to a sample whose size is much larger than the average grain radius. To simulate the solidification of the small DSC specimens, a modified version of a three-dimensional stochastic model, previously developed for eutectic alloys, was used (9). It was specifically applied to the isothermal solidification of the spherulites of γ-POP at 15°C. The principle of this model is as follows: in a sample of pure POP of the size of the DSC pan, maintained at constant temperature, the nuclei are all activated at time $t = 0$. The grain density is deduced from the experimental observations, and the centers of nucleation are randomly selected in the volume of the sample. The crystals then grow spherically with a constant growth rate deduced from Figure 5. Therefore, all grains have the same radius. The model tracks the impingement of the grains between each other or with the surface of the specimen by subdividing the interface of each grain into a certain number of facets of nearly equal surface and by detecting which of these facets are still in contact with the liquid. Therefore, the model is able to calculate the effective solid–liquid surface, the volume fraction of solid, the associated latent heat released in the sample, and it allows to directly visualize the grain structure in three dimensions, in two-dimensional cuts or in projection.

The results of this model with data: melting temperature, 23.9°C; solidification temperature, 15°C; latent heat, 10^8 J/m^3; growth rate, 0.28 μm/s; nuclei density, 1.2 10^{13} m^3; size of window of observation, 0.65 • 0.496 mm^2; sample height, 50 μm; number of facets for each grain, 732, are compared in Figure 7 with PLM observations of POP spherulites, formed isothermally at 15°C. The comparison is made for four successive times of solidification, the time $t = 0$ being set at crystallization start (i.e., at the start of the DSC peak on the isothermal plateau). The grains in the simulation (right of Fig. 7) are shown in white, whereas the liquid is black. The experimental and simulated grain structures are in fact projections of the largest sections of all grains and not transversal cuts of the sample; they show a false view of the microstructure and overestimate the volume fraction of solid. The stochastic model provides a realistic description of grain structure formation. It also gives the evolution of the latent heat released by the grains, which is compared with the DSC peak measured in Figure 8. The agreement of the two peaks is excellent, especially if one considers the assumption made for the nucleation rate.

As a conclusion, TTT diagrams were measured for the three TAG, and then were used with our model under non-

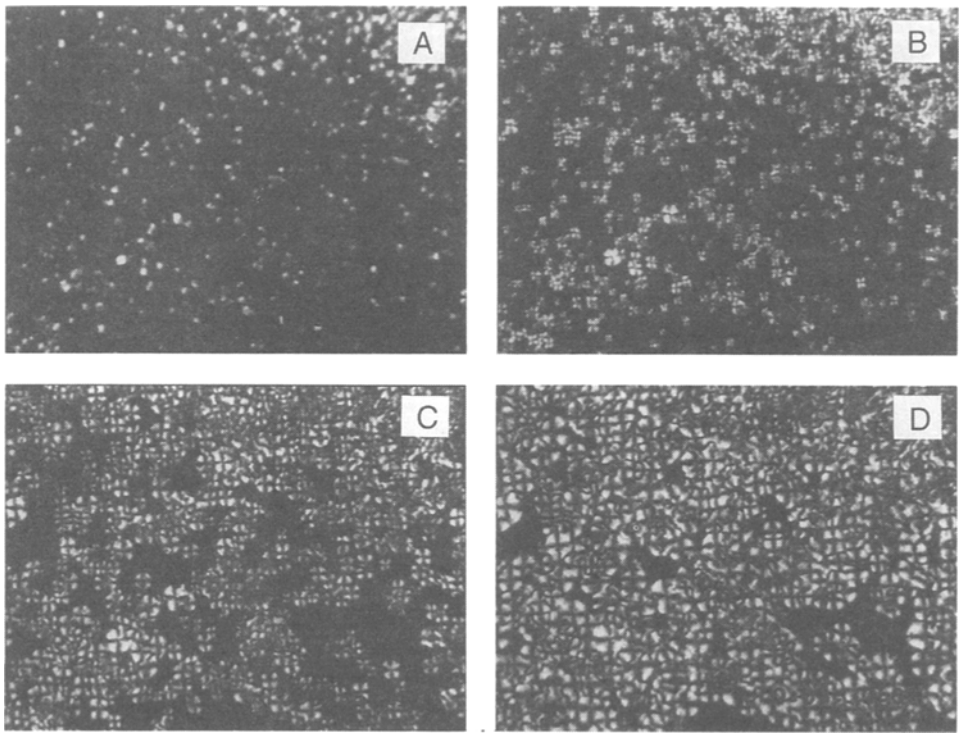

FIG. 7. Experimental (left) and simulated (right) polarized light microscopy views of a POP sample solidifying at 15°C, at different times. Abbreviations as in Figures 1 and 2.

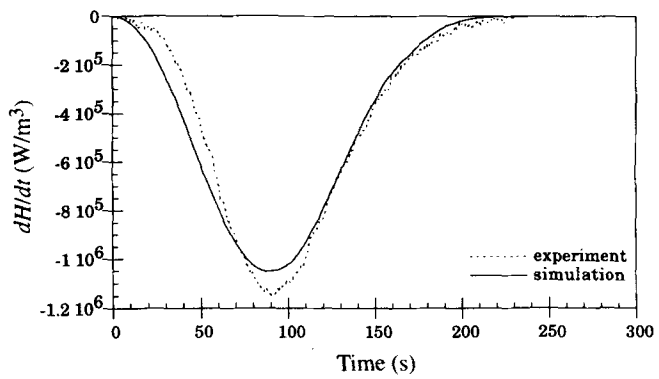

FIG. 8. Comparison between the experimental and the simulated differential scanning calorimetry peaks of POP solidifying at 15°C. Abbreviations as in Figures 1 and 2.

isothermal conditions. Such an approach could be extended to more complex crystallization conditions. The second model, closer to the mechanisms of nucleation and growth of the phases, can provide a better vision of the phenomena involved when the grain morphology is simple.

ACKNOWLEDGMENTS

The authors thank the Commission pour l'Encouragement de la Recherche Scientifique (CERS), Bern, Switzerland, and the Nestlé Research Center, Vers chez les Blanc, for their support (CERS project 2944.1). The encouragement of Dr. Löliger and the helpful discussions with Drs. C. Bertoli and E. Minner, from Nestlé Research Center, are also gratefully acknowledged.

REFERENCES

1. Manning, D.M., and P.S. Dimick, Crystal Morphology of Cocoa Butter, *Food Microstructure 4*:249–265 (1985).
2. Seguine, E.S., Tempering the Inside Story, *Manufacturing Confectioner 71*:117–125 (1991).
3. Jeffery, M.S., Molding Technology, *Ibid. 67*:67–69 (1987).
4. Garti, N., and Sato, K. (eds.) *Crystallization and Polymorphism of Fats and Fatty Acids*, Surfactant Science Series, Vol. 31, Marcel Dekker, Inc., New York, 1988, pp. 3–137.
5. Koyano, T., I. Hachiya, T. Arishima, K. Sato, and N. Sagi, Polymorphism of POP and SOS. II. Kinetics of Melt Crystallization, *J. Am. Oil Chem. Soc. 66*:675–679 (1989).
6. Koyano, T., I. Hachiya, T. Arishima, N. Sagi, and K. Sato, Polymorphism of POS. II. Kinetics of Melt Crystallization, *Ibid. 68*:716–718 (1991).
7. Porter, D., and K. Easterling (eds.) *Phase Transformations in Metals and Alloys*, Van Nostrand Reinhold Company, 1981, pp. 287–290.
8. Avrami, M., Kinetics of Phase Change, I and II, *J. of Chem. Physics 7*:1103–1113 (1939); *8*:212–224 (1940).
9. Charbon, Ch., A. Jacot, and M. Rappaz, 3D Stochastic Modelling of Equiaxed Solidification in the Presence of Grain Movement, *Acta Metall. Mater. 42*:3953–3966 (1994).
10. Larson, K., On the Structure of the Liquid State of Triglycerides, *Acta Chem. Scand. 20*:2255–2255 (1966).
11. Sato, K., T. Arishima, Z.H. Wang, K. Ojima, N. Sagi, and H. Mori, Polymorphism of POP and SOS. I. Occurrence and Polymorphic Transformation, *J. Am. Oil Chem. Soc. 66*:664–674 (1989).
12. Arishima, T., N. Sagi, H. Mori, and K. Sato, Polymorphism of POS. I. Occurrence of Polymorphic Transformation, *Ibid. 68*:710–715 (1991).
13. Eder, G., H. Janeschitz-Kriegl, and S. Liedauer, Crystallisation Processes in Quiescent and Moving Polymer Melts Under Heat Transfer Conditions, *Prog. Polym. Sci. 15*:629–714 (1990).
14. Rappaz, M., Modelling of Microstructure Formation in Solidification Processes, *Int. Material Review 34*:93–123 (1989).
15. Dimick, P.S., and D.M. Manning, Thermal and Compositional Properties of Cocoa Butter During Static Crystallization, *J. Am. Oil Chem. Soc. 64*, 1663–1669 (1987).
16. Kellens, M., W. Meeussen, and H. Reynaers, Study of the Polymorphism and the Crystallization Kinetics of Tripalmitin: A Microscopic Approach, *Ibid. 69*:906–911 (1992).
17. Denis, S., D. Farias, and A. Simon, Mathematical Model Coupling Phase Transformations and Temperature Evolutions in Steels, *ISIJ Int. 32*:316–325 (1992).
18. Charbon, C., and M. Rappaz, Shape of Grain Boundaries During Phase Transformations, *Acta Metall. Mater.*, in press (1996).
19. Sharples, A., Crystallinity, in *Polymer Science*, edited by A.D. Jenkins, North-Holland Publishing Company, 1972, pp. 251–321.
20. Ovsienko, D., and G. Alfintsev, Growth and Properties, in *Crystals, 2, Growth, Properties and Applications*, Springer-Verlag, Berlin, 1980, pp. 118–169.
21. Jacot, A., M. Swierkosz, J. Rappaz, M. Rappaz, and D. Mari, Mechanisms and Mechanics of Solid-Solid Phase Transformations, Proceeding of Mecamat 95, *le Journal de Physique*, in press (1996).

[Received December 5, 1995; accepted March 21, 1996]